Ultra small-angle X-ray scattering: conditions, limits and results in speckle experiments

Frédéric Livet,[a]* Françoise Bley,[a] Françoise Ehrburger-Dolle,[b] Erik Geissler,[b] David Lebolloc'h[c] and Tobias Schulli[d]

[a]LTPCM (UMR-CNRS 5614), INPG/UJF, BP 75, 38402 St Martin d'Hères, France, [b]LSP (UMR-CNRS 5548), Université J. Fourier, BP 87, 38402 St Martin d'Hères, France, [c]LPS (UMR-CNRS 8502), Université Paris-Sud, Bat. 510, 91405 Orsay cedex, France, [d]ESRF, European Synchrotron Radiation Facility, BP 220, 38043 Grenoble Cedex France. E-mail: flivet@ltpcm.inpg.fr

To carry out small-angle scattering experiments with X-rays in the scattering vector range $q < 10^{-3}$ Å^{-1} with area detectors, background must be carefuly reduced. The principal source of background is slit scattering. Careful polishing of slits allows slit diffraction to be observed, which can be calculated from wave equations. In this case, the background takes the shape of thin streaks perpendicular to the slit edges. This introduces the design of new beamstops, which are cross-shaped. Typical results obtained on the D2AM beamline of the ESRF are shown, especially for the case of coherent scattering.

Keywords: ultra small-angle setups; CCD area detectors; coherent X-ray beams; slits diffraction.

1. Introduction

Small angle X-ray scattering (SAXS) experiments on synchrotron sources make new experiments possible for the exploration of matter. The X-ray source has a very small size and at the same time is highly directional, thus giving a brilliance that is about ten orders of magnitude larger than for classical sources. This opens new possibilities for experiments in the domain of very small angles, of time-resolved measurements and in the domain of coherent X-ray measurements (Sutton *et al.*, 1991).

These measurements are strongly dependent on the development of area detectors, where intensity is collected over a plane in reciprocal space. Such detectors are essentially based on CCD cameras. We shall distinguish between "indirect" detection (a fluorescent screen and an optical setup driving secondary photons to the CCD chip) and "direct" detection, where X-rays are absorbed by the chip.

Both types of detector are used on the D2AM beamline at the ESRF (French CRG, on a bending magnet beamline). This beamline is highly flexible, and many experiments involve the domain of very low angles, especially for soft condensed matter (SCM) systems (Rigacci *et al.*, 2001). The beamline has been modified in order to produce a coherent beam (Livet *et al.*, 1998) and to make photon correlation spectroscopy (PCS) measurements in the domain of X-rays (Geissler *et al.*, 2000). One of the goals was to obtain measurements in a q domain that extends over the range of standard visible light scattering, and to compare results with light PCS experiments. This technique also provides results on optically opaque samples.

The domain of interest here ranges from $q = 4 \times 10^{-4}$ to $q = 4 \times 10^{-3}$ Å^{-1}, which we define as USAXS (ultra-SAXS). Here q is the modulus of the scattering vector, $4\pi \sin\theta/\lambda$, θ is half the scattering angle and λ is the wavelength of the incident beam. In this very low angle region (down to 100 μradians in the angle 2θ), the reduction of background in the vicinity of the direct beam is essential, especially when CCD-based detectors are used, where pixel saturation must be avoided.

We have carried out experiments in this q range on various beamlines at the ESRF (ID10, ID20, ID1, D2AM), and we have found difficult to reduce experimental background. For this reason, a systematic study was tempted in order to clarify the origin of parasitic scattering and to improve the experimental setups. In this paper, we discuss various methods that we have developed for these experiments, with typical results from the ID1 and D2AM beamlines to illustrate the discussion.

2. Description of the D2AM beamline

2.1. Optics

The optical setup has been described in a previous paper (Simon *et al.*, 1997). The main elements of our flexible optics are the secondary mirror for vertical focusing and the second monochromator for horizontal focusing. The source to optics distance is 27 m and the optics to sample distance is 10 m.

According to the data given by the ESRF databooks, the source sizes are $\sigma_v = 30$ μm and $\sigma_h = 77$ μm (RMS). From the distance ratio given above (2.7) and using the factor 2.35 between FWHM and RMS, the size of a perfectly focused beam is : 26 μm $\times$ 67 μm (width $\times$ height, FWHM).

Unfortunately, the optics of D2AM was investigated for a focal point of the order of 200 μm, in accordance with the initial specifications of the ESRF.

The 1 m long mirrors have FWHM slope errors of about 10 μradians, which correspond to a focal spot of $\simeq$ 200 μm vertically. In practice, when this focus is carefully examined with a high resolution camera, a set of horizontal lines is observed, due to the "wavy" surface of our mirrors. From these images, we found regions of better quality on the mirror.

Horizontally, the focusing crystal has ribs with a period of 1.4 mm, and a periodic bending is observed. When this crystal is underfocused, a set of spots is obtained, corresponding to the well focused space between ribs, with a period of 300 μm. At higher crystal bending, all spots are confused in a 250 μm focal spot. By selecting a region between two ribs, much better focus can be obtained.

2.2. Parameters

Main parameters for USAXS are:
-The size of the beam ϕ and its angular divergence ϵ.
-The sample to detector distance: $D < 2.4$ m, in the case of the D2AM experiment
-The beamstop size h
-The detector resolution d.

For typical USAXS experiments on the D2AM beamline, the primary slits at the optics limit the beam dimensions to 0.6 mm $\times$ 0.6 mm, and the focus in this case is 40 μm $\times$ 80 μm (FWHM) close to the sample position. This compares well with the theoretical estimations given above. The beam divergence is: $\epsilon = 60$ μradians. In this case, the beam intensity is about 10^9ph/s, and the beam dimension (FWHM) in the vicinity of the beamstop is $\simeq$ 140 μm. For practical experiments, primary slits and beam limiting slits before the sample near the focal point have to be adjusted. The beam intensity is then reduced by a factor corresponding to the surface of the slits.

All results described in this paper were obtained with the direct illumination CCD detector, used as a photon counting detector as decribed in Ref. (Livet *et al.*, 2000). This detector has very good resolution (22

μm), but it has a small size (384 $\times$ 576 pixels), which gives only a small range in q-space.

3. Background

In order to reduce background, our beamline is evacuated. All windows after the optics have been eliminated, except for certain SCM samples where two mica windows are added to contain the sample. Such mica windows introduce negligible parasitic scattering. Slits are necessary in the vicinity of the sample because the focused beam has to be free from optical defects. These are induced by imperfections of our mirrors, but also by unpolished beryllium windows that are still present in the optics.

3.1. Slit scattering

With the background reduction precautions now currently used: evacuated beamline, mica windows, polished beryllium windows..., we have observed that slit parasitic scattering is now the principal cause of experimental background. We will mainly discuss slit diffraction, though some reflection can also occur at the surface of slit edges.

In order to introduce this problem, we give two images in Fig. 1 of slits of aperture of a few micrometers. These were obtained on the (Lebolloc'h *et al.*, 2002) beamline ID1 during tests of slits. In Fig. 1(*a*), the edges were standard tungsten blades; in Fig. 1(*b*), the edges were replaced by carefully polished tantalum cylinders.

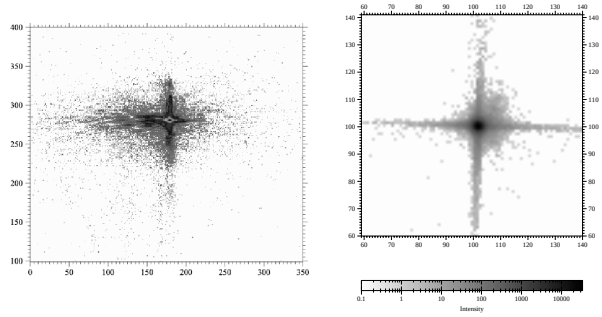

(*a*) (*b*)

Figure 1
Scattering observed with (*a*) unpolished edges, (*b*) polished cylindrical edges. Each pixel of the CCD corresponds to $\Delta q = 5 \times 10^{-5}$ Å^{-1}, slit aperture: 10 μm $\times$ 10 μm.

The second image can be compared with intensity calculations from wave propagation. For large angles, streaks are observed perpendicular to the slit edges. The ratio of the total background intensity (isotropically averaged) for $q > q_0$ to the beam intensity can be estimated as $l/\pi s q_0$ Here, l is the length of the slit edges (4ϕ in the case of square aperture of size ϕ), and s is the aperture area (ϕ^2 in the case of square slits).

Beam limiting slits are often used, either to "clean" the beam, or to obtain a beam of small size (coherent or otherwise). If 50 μm aperture slits are used for limiting the beam, the total background intensity in our experiment for $q_0 = 4 \times 10^{-4}$ Å^{-1} is of the order of 1%.

3.2. Guard slits

Guard slits are currently used in SAXS experiments to reduce background. Here, the parasitic scattering increases for small apertures. This is directly related to slit diffraction. This makes necessary the use of more complex setups, with guard slits, the effect of which should also be discussed from the point of view of wave propagation.

Such a setup can be represented schematically as second slits, of aperture ϕ', at a distance D after the beam limiting slits. Within some assumptions, the reduction in background (Lebolloc'h *et al.*, 2002) is of the order of $(\lambda D/\phi\phi')^2$ For $\lambda \simeq 1.6$ Å, $D \simeq 1$ m and $\phi \simeq 50$ μm, $\phi' \simeq 200$ μm, the background is reduced by a few thousand. Moreover, wave calculations show that the remaining background intensity is strongly concentrated into streaks perpendicular to the slit edges.

We can exploit this property, provided that care is taken with the guard slits. Fig. 2(*a*) shows the result obtained with unpolished guard slits. The beamstop is here a 0.5mm diameter lead disk. Irregular scattering from unpolished cylindrical slits are observed. After polishing the tantalum cylinders of our guard slits, the background was concentrated into thin streaks, and a new beamstop was used, made of two perpendicular platinum wires. In Fig. 2(*b*), the background is strongly reduced, except in the two directions perpendicular to the guard slit edges. A 300 μm Pt wire was used as beamstop.

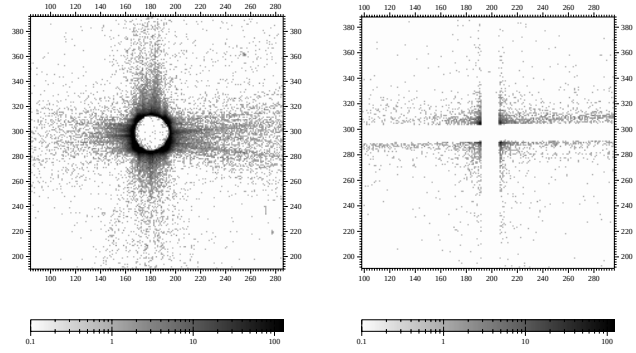

(*a*) (*b*)

Figure 2
Scattering with guard slits. Sample-detector distance 2.2 m, pixel size 22 μm, $\Delta q = 4 \times 10^{-5}$ Å^{-1} per pixel of the CCD. (*a*) unpolished edges, disk-shaped beamstop 500 μm diameter (*b*): polished cylindrical edges, crossed beamstop of 300 μm wires

Both these figures were obtained with beam intensities of the order of 10^6 ph/s and with the direct illumination CCD detector. The photon counting technique described in (Livet *et al.*, 2000) was used. In both cases, the acquisition time was 200 s, the units are counts per pixel and the detector quantum efficiency is about 50%.

4. Some results

4.1. USAXS anisotropic measurements

Area detectors in SAXS measurements open the possibility of observing anisotropic scattering. The q range discussed in this paper corresponds to the size of moving inclusions in rubber composites when a stress is applied. For this purpose, an "in situ" setup for applying stress to samples has been used on the D2AM beamline.

In Fig. 3, typical results obtained are shown. The sample is a carbon black- elastomer composite, where the polymer is uncross-linked. Anisotropy in the scattering is observed. In this figure, stress corresponds to the horizontal direction. In this direction, and also in the perpendicular direction, the cross-shaped beamstop blinds a part of the CCD. Fig. 4 shows the directional intensities averaged over angles of $\pm 15°$. In this case, results are obtained only for $q > 6 \times 10^{-4}$ Å^{-1}.

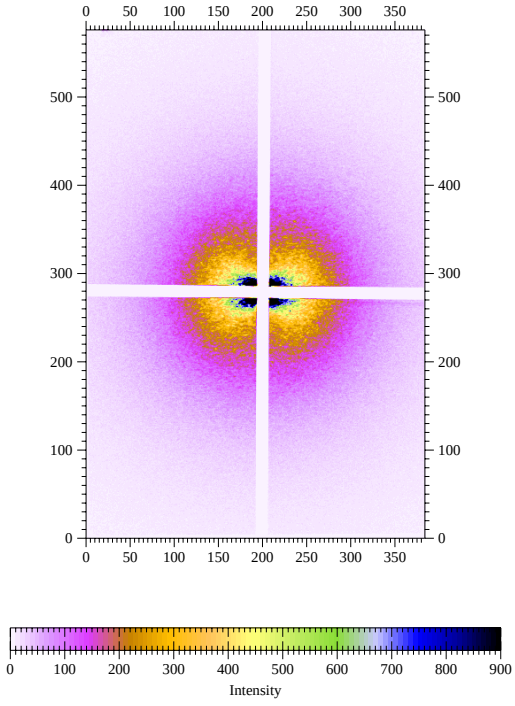

Figure 3
Scattering observed with an "in situ" stretched sample (Carbon black in an elastomer, stress is applied horizontally). $\Delta q = 4 \times 10^{-5}$ Å^{-1} per pixel

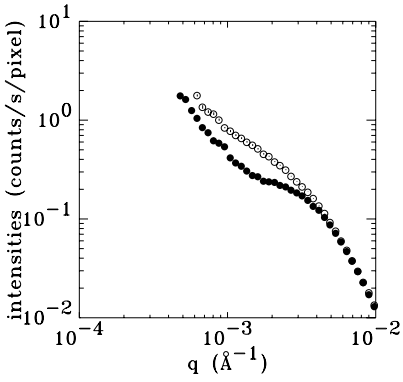

Figure 4
Angular dependence of SAXS from the results of Fig. 3. ○ : parallel to stress, ● : perpendicular to stress. The anisotropy is observed in the 5×10^{-4} to 5×10^{-3} Å^{-1} range

Clearly, these improvements in the USAXS domain appear very promising for SCM systems, because many "mesoscopic" phenomena can be observed in this q range (Ehrburger-Dolle *et al.*, 2001).

4.2. X-ray photon correlation spectroscopy

Among new methods available at synchrotrons, the use of coherent beam appears as a new field. Obtaining a coherent beam is simply a natural limit of high resolution experiments: the beam must be in the vicinity of the diffraction limit: $\epsilon\phi \simeq \lambda$ The necessary resolution of the detector is of the order of the angular diffraction of the ϕ apertures: λ/ϕ, in the 10 μradians range. In practice, for an incident wavelength of 1.6 Å, we need $\epsilon \simeq 10$ μradians and $\phi \simeq 10$ μm. For the D2AM beamline, the primary slits are closed to 200 μm and a $\phi = 10$ μm diameter circular pinhole is used. The detector has a resolution of 22 μm and is placed at a distance of 2.2 m, providing good angular resolution. The beam intensity is between one and two 10^6 ph/s for a storage ring current of 200 mA. The pinhole-guard slits distance is 0.17 m and aperture of the guard slits is $\phi' \simeq 20$ μm.

For a static test sample, like silica aerogel, we observe a speckle structure in the detector, as shown in Fig. 5. For a dynamic sample, the time changes in speckle structure are recorded.

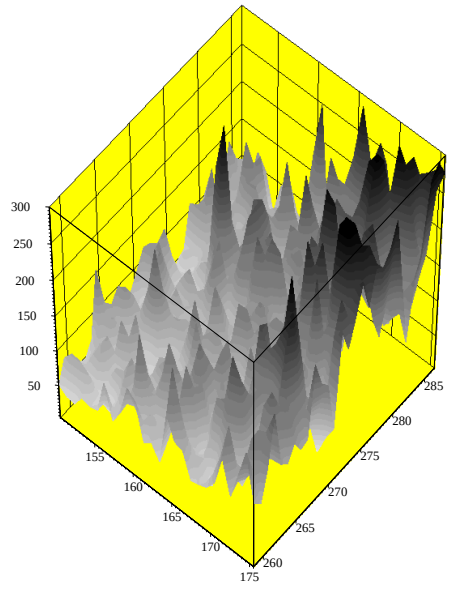

Figure 5
A small part of the CCD detector showing the speckle structure with a static silica aerogel sample. $\Delta q = 4 \times 10^{-5}$ Å^{-1} per pixel

The dynamics of the movement of inclusions in a SCM sample can be deduced from the study of the correlations (Geissler *et al.*, 2000):

$$1 + \gamma(t,q) = < I(q,t+t')I(q,t') > / < I(q,t') >^2 \qquad (1)$$

where $<>$ corresponds to averages over t' and over the set of pixels having the same q. This latter average is the main reason for using area detectors in the case of PCS in X-rays, and is carried out in a domain where angular variations of the non-coherent scattering can be neglected. The large number of pixels partially compensates for low intensities. The function $\gamma(t,q)$ can be written as:

$$\gamma(t,q) = \beta\alpha(t,q) \qquad (2)$$

where β is the coherence factor, varying from 0 (no coherence) to 1 (full coherence). In our SAXS q domain, with the Si_{111} monochromatic beam, β is q-independent. $\alpha(t,q)$ is a measure of the q-dependent relaxation of the system under study.

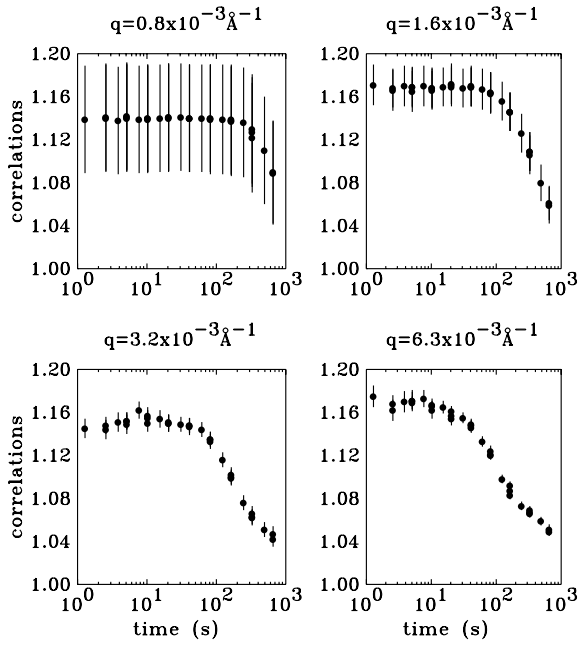

Figure 6
Time correlations (as defined in equation 1) observed for various values of q, showing the relaxations of the same system as in Fig. 3, before stretching: isotropic scattering

In a simple theory of relaxation, based on diffusion processes (Geissler *et al.*, 2000),(Brown, 1993), $\alpha(t,q) = \exp(-t/\tau(q))$, with $\tau(q) = 1/Dq^2$.

In the case studied, corresponding to the system of Fig. 3 before being streched, Fig. 6 shows some correlations obtained for various q values. In these figures, time is in logarithmic units. One can estimate that in this experiment, $\beta \simeq 0.17$ (time zero intercept) and that the relaxation time varies from 900 s ($q = 0.8 \times 10^{-3}$ Å^{-1}) to 150 s ($q = 6.3 \times 10^{-3}$ Å^{-1}).

5. Discussion

Obviously, the system studied in Fig. 6 does not correspond to the standard diffusion model. These results are used to illustrate the typical possibilities of the XPCS technique with a bending magnet at the ESRF. Only systems with strong scattering and long fluctuation times give results of reasonable precision. Our SAXS setup is mounted on a very stable granite bench. This, together with the high stability of the optics, makes possible long measurements: hours without any change of the speckle structure of a static sample. The main observed instability is a slow 20 μm change of the focal point of our optics over a period of 24 hours.

We observe here that calculating the background from first principles using wave propagation theory is a valuable means of improving experiments. For instance, it can be shown that the current distance between pinhole and guard slit (0.17 m) is too small. We estimate that if this distance were doubled, smaller q-values could be obtained (close to $2-3\times10^{-4}$ Å^{-1}), at least for coherent scattering experiments, i.e., the micrometer range in real space.

From our experiments, we observe that poor focusing produces an irreversible degradation in the source brilliance. For instance, the vertical size of an ESRF undulator source is 8 μm (RMS), and a well focused image should be in the range of 10 μm (FWHM). In practice, it often reaches hundreds of μm! It follows that a factor 10 (at least) is lost. For this reason, it would seem to be more rewarding to improve the X-ray optics than to develop new undulators. Such an improvement probably requires shorter mirrors, of better quality.

The authors want to thank all the D2AM team for numerous collaborations, especially Jean-Paul Simon, Jean-François Bérar, Stephan Arnaud and Bernard Caillot. We also thank Andy Hammersley from ESRF for providing the program fit2d.

References

Brown, W. (ed.) (1993). *Dynamic Light Scattering, The method and some applications*, chap. 11. Oxford: Clarendon Press.

Ehrburger-Dolle, F., Hindermann-Bischoff, M., Livet, F., Bley, F., Rochas, C. & Geissler, E. (2001). *Langmuir*, **17**, 329–343.

Geissler, E., Hecht, A. M., Rochas, C., Bley, F., Livet, F. & Sutton, M. (2000). *Phys. Rev.* E**62**, 8308–8313.

Lebolloc'h, D., Livet, F., Bley, F., Schulli, T., Veron, M. & Metzger, T. H. (2002). *J. Synchr. Rad.* **9**, 258–265.

Livet, F., Bley, F., Létoublon, A., Simon, J. P. & Bérar, J. F. (1998). *J. Synchr. Rad.* **5**, 1337–1345.

Livet, F., Bley, F., Mainville, J., Sutton, M., Mochrie, S., Geissler, E., Dolino, G., Abernathy, D. & Gruebel, G. (2000). *Nucl. Instr. Meth.* A**451**, 596–609.

Rigacci, A., Ehrburger-Dolle, F., Geissler, E., Chevalier, B., Sallée, H., Achard, P., Barbieri, O., Berthon, S., Bley, F., Livet, F., Pajonk, G., Pinton, N. & Rochas, C. (2001). *J. Non-cryst. solids*, **285**, 187–193.

Simon, J. P., Arnaud, S., Bley, F., Bérar, J. F., Caillot, B., Comparat, V., Geissler, E., Degeyer, A., Livet, F. & Okuda, H. (1997). *J. Appl. Cryst.* **30**, 900–904.

Sutton, M., Mochrie, S. G. J., Greytak, T., Nagler, S. E., Berman, L. E., Held, G. A. & Stephenson, G. B. (1991). *Nature*, **352**, 608–609.

 Received 29 August 2002 • Accepted 3 January 2003